Mass estimations of ejecta from Strombolian explosions by inversion of Doppler radar measurements

Mathieu Gouhier, Franck Donnadieu

Mass estimations of ejecta from Strombolian explosions by inversion of Doppler radar measurements

Mathieu Gouhier[1] and Franck Donnadieu[1]

Received 13 September 2007; revised 25 June 2008; accepted 23 July 2008; published 4 October 2008.

[1] We present a new method for estimating particle loading parameters (mass, number, volume) of eruptive jets by inversion of echo power data measured using a volcano Doppler radar (VOLDORAD) during typical Strombolian activity from the southeast (SE) crater of Mount Etna on 4 July 2001. Derived parameters such as mass flux, particle kinetic and thermal energy, and particle concentration are also estimated. The inversion algorithm uses the complete Mie (1908) formulation of electromagnetic scattering by spherical particles to generate synthetic backscattered power values. In a first data inversion model (termed the polydisperse model), the particle size distribution (PSD) is characterized by a scaled Weibull function. The mode of the distribution is inferred from particle terminal velocities measured by Doppler radar for each explosion. The distribution shape factor is found to be 2.3 from Chouet et al.'s (1974) data for typical Strombolian activity, corresponding to the lognormal PSDs commonly characteristic of other Strombolian deposits. The polydisperse model inversion converges toward the Weibull scale factor producing the best fit between synthetic and measured backscattered power. A cruder, alternative monodisperse model is evaluated on the basis of a single size distribution assumption, the accuracy of which lies within 25% of that of the polydisperse model. Although less accurate, the monodisperse model, being much faster, may be useful for rapid estimation of physical parameters during real-time volcano monitoring. Results are illustrated for two explosions at Mount Etna with contrasted particle loads. Estimates from the polydisperse model give 58,000 and 206,000 kg as maxima for the total mass of pyroclasts, 26,400 and 73,600 kg s^{-1} for mass flux rates, 38 and 135 m^3 (22 and 76 m^3 equivalent magma volume) for the pyroclast volumes, and 0.02–0.4 and 0.06–0.12 kg m^{-3} for particle concentrations, respectively. The time-averaged kinetic energy released is found to be equal to 4.2×10^7 and 3.9×10^8 J, and thermal energy is estimated at 8.4×10^{10} and 3×10^{11} J.

Citation: Gouhier, M., and F. Donnadieu (2008), Mass estimations of ejecta from Strombolian explosions by inversion of Doppler radar measurements, *J. Geophys. Res.*, *113*, B10202, doi:10.1029/2007JB005383.

1. Introduction

[2] Volcanic explosions are important sources of information for understanding eruption mechanisms. The masses and velocities of gas and pyroclasts are particularly important parameters controlling the dynamics of an eruption as they define crucial parameters such as mass fluxes, kinetic and thermal energies released by an explosion. In order to better understand the dynamics of explosive eruptions, satellite imagery, and ground-based weather radars particularly have been used for the sounding of volcanic ash plumes from large eruptions [*Harris et al.*, 1981; *Harris and Rose*, 1983; *Weill et al.*, 1992; *Dean et al.*, 1994; *Dehn et al.*, 2000; *Lacasse et al.*, 2004]. These techniques probe the upper convective parts of high eruption columns and provide information primarily on the small particles that ultimately constitute the distal volcanic products. A major challenge is now to measure physical parameters, such as ejecta velocities and masses, close to the vent in order to retrieve directly the true source parameters. A first approach to measure jet velocities was used at Stromboli with an acoustic Doppler sounder (sodar) [*Weill et al.*, 1992]. Other techniques that potentially provide information on both velocity and mass parameters are ground-based portable Doppler radar, either pulsed such as volcano Doppler radar (VOLDORAD) [*Dubosclard et al.*, 1999; *Dubosclard et al.*, 2004] or frequency-modulated such as VERDEMOS [*Hort and Seyfried*, 1998; *Seyfried and Hort*, 1999]. These techniques allow direct measurement of particle velocities and reflectivities immediately above the vent. In addition to their significant monitoring potential, these radar systems allow us to study, under any weather conditions, explosions

[1]Laboratoire Magmas et Volcans, Clermont-Université, Observatoire de Physique du Globe de Clermont-Ferrand, Clermont-Ferrand, France.

0148-0227/08/2007JB005383$09.00

Table 1. Characteristics of VOLDORAD Version 2

Characteristic	Symbol	VOLDORAD 2
Transmitted frequency (MHz)	f_t	1274
Wavelength (cm)	λ	23.5
Peak power (W)	P_t	60
Pulse repetition period[a] (μs)	t_r	100
Pulse duration[a] (μs)	τ	0.8
Range resolution[a] (m)	L	120
Antenna beam width (deg)	α	9
Antenna beam elevation[a] (deg)	θ	23

[a]Parameters set for the sounding at Etna SE crater on 4 July 2001.

of lesser intensity barely imaged by satellites or weather radars.

[3] VOLDORAD was used to record several eruptive episodes at Etna in July 2001, ranging from mild Strombolian activity to paroxysmal lava fountains [*Donnadieu et al.*, 2005]. A new method based on inversion of echo power data measured using VOLDORAD is now presented for estimating the masses of pyroclasts ejected during individual explosions. The method also provides first-order estimates of mass-related parameters such as mass flux, ejecta volume, particle concentration, thermal and kinetic energy at the vent. The method was applied to two Strombolian explosions with contrasted particle loads that occurred during an eruptive episode of Mount Etna southeast (SE) crater on 4 July 2001. First, an algorithm is developed to simulate radar echoes from pyroclasts of various sizes, using the complete electromagnetic scattering formulation [*Mie*, 1908]. This approach provides synthetic data of power backscattered by particles (P_{synth}) at the particular wavelength employed by VOLDORAD. Second, as an input to the model, a scaled Weibull function [*Weibull*, 1939] is used to characterize the particle size distribution (PSD). The general shape of the Weibull distribution is constrained from published data for typical Strombolian activity [*Chouet et al.*, 1974], and the mode of the PSD is estimated from our own radar velocity measurements for each explosion. All Weibull parameters characterizing a polydisperse (multiple particle size) distribution, such as shape, shift, and scale factors, can then be deduced and used to compute synthetic values of backscattered power. Last, a recursive inversion algorithm is applied in order to obtain a PSD such that the synthetic power (P_{synth}) best fit the measured radar power (P_{mes}). The mass of ejected material and related parameters are then deduced. An alternative model is proposed on the basis of a monodisperse (single particle size) PSD, which turns out to be an acceptable approximation of the polydisperse model. This approach reduces computing time, making it useful for real-time quantitative assessment of ejected mass during volcano monitoring.

2. VOLDORAD: Volcano Doppler Radar

2.1. Radar Description

[4] VOLDORAD is a pulsed volcano Doppler radar developed by the Observatoire de Physique du Globe in Clermont-Ferrand (France) specifically for the active remote sensing of volcanic eruption jets and plumes. The second version of the system is a medium-power (60 W) Doppler radar of limited weight ($\sim$70 kg, including PC and antenna), with a 9° beam width (α) and a working wavelength (λ) of 23.5 cm [*Donnadieu et al.*, 2005]. VOLDORAD is designed to monitor all types of explosive volcanic activity of variable magnitude. It operates at a medium distance range (0.4–12 km) under all weather conditions with a high sampling rate ($\geq$10 Hz) that permits detailed analysis of early eruptive processes. The portability and lower electric consumption of this version compared to a first version of VOLDORAD is a valuable technical improvement. The pulse repetition period (t_r) is taken as 100 μs and directly defines the maximum velocity that can be measured by the radar:

$$V_{\max} = \frac{\lambda}{4N_c t_r} \tag{1}$$

where N_c is the number of coherent integrations of radar pulses. Note that the maximum velocity that can be measured in theory by VOLDORAD is very high (1175 m/s). This is valuable in particular for measuring the velocities of small particles traveling with speeds close to that of the gas. The pulse duration (τ) can be varied from 0.4 to 1.5 μs, and a value of 0.8 μs was used during the eruption of Mount Etna SE crater on 4 July 2001. This corresponds to a suitable range resolution of the sampling volume, the so-called range gate, of 120 m (Table 1).

[5] Volcanic ejecta crossing the antenna beam generate radar echoes backscattered to the receiver with an angular frequency Doppler shift ($d\varphi/dt$) between the transmitted and received signal that is related to the particle velocity along the beam axis:

$$\frac{d\varphi}{dt} = \omega = 2\pi f_d \tag{2}$$

where ω is the angular frequency and f_d is the Doppler frequency. Indeed, the Doppler velocity spectrum is related to the frequency spectrum via the relationship

$$f_d = \frac{-2V_r}{\lambda} \tag{3}$$

where V_r is the radial velocity and λ is the radar wavelength. When the target moves away from the radar ($V_r > 0$), the Doppler shift ($d\varphi/dt$) is negative, and vice versa when the target approaches.

2.2. Experimental Conditions

[6] After more than 8 months of minor activity (slow lava flows, degassing, light ash emission, and low-level Strombolian activity), a new episode of vigorous activity began at the SE crater on 9 May. From then until July–August 2001, there were eruptions from the SE crater every 3–5 days, each lasting on average a few hours and involving multiple Strombolian explosions and lava fountaining. Radar soundings reported here were carried out over about 5 h during an eruption on 4 July. The activity began at about 1800 UT and at first involved small explosions repeated every $\sim$10 s. The intensity then increased progressively, culminating in very powerful Strombolian explosions every 2–3 s, with the bursting of very large bubbles between 2100 UT and 2200 UT but without real lava fountains. The eruption intensity then decreased rapidly from 2200 UT and ended at 2300 UT after about 5 h of Strombolian activity.

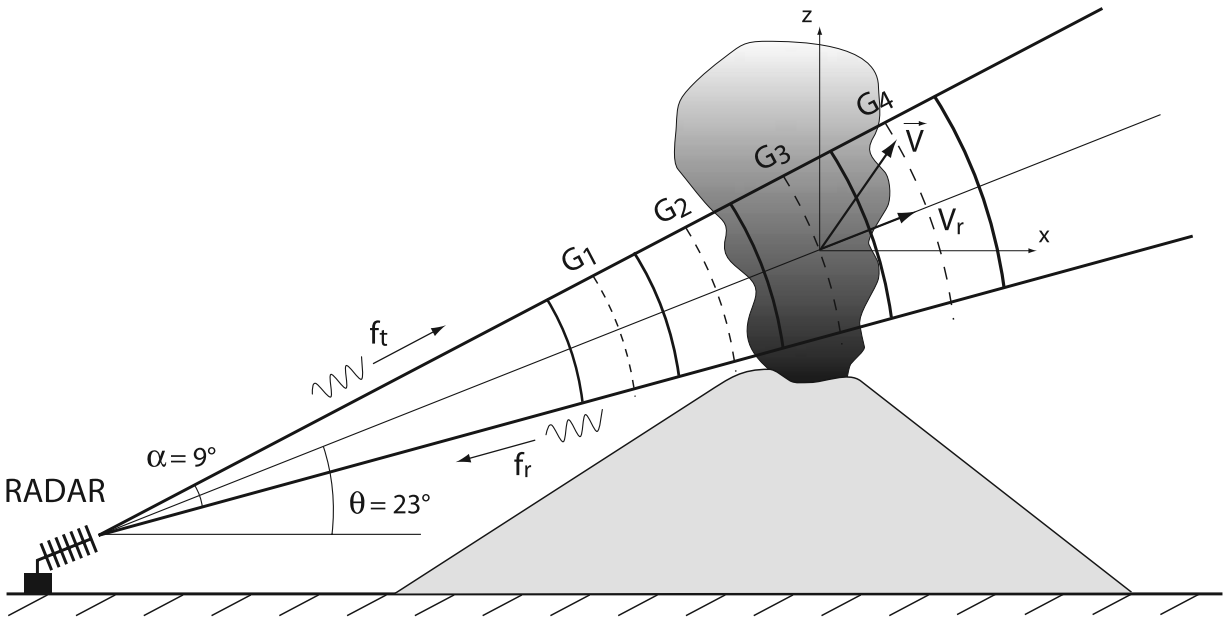

Figure 1. Sketch of the radar sounding geometry used for the acquisition campaign on Mount Etna, on 4 July 2001. VOLDORAD was set up at an altitude of 3000 m, at a slanting distance of 930 m to the crater rim, 280 m below the summit of the SE crater, and with an antenna elevation angle θ of 23°. Note that range gate G_3 is centered above the vent and provides most of the echo power.

VOLDORAD was set up at an altitude of 3000 m, at a slanting distance of 930 m to the crater rim, 280 m below the summit of the SE crater, and with an antenna elevation angle θ of 23° (Figure 1).

[7] Moving particles were detected in successive range gates (G_1 to G_4) corresponding to a slant distance of 807–1167 m (Table 2). In this configuration, particles ascending above the crater in range gate G_3 were recorded mainly with positive radial velocities (away from the antenna) in the Doppler spectra, whereas descending particles were mainly recorded with negative velocities.

2.3. Radar Parameters

[8] Data from successive range gates are displayed in real time as Doppler spectra representing the power spectral density versus radial velocity. From the processing of the series of Doppler spectra, two sets of parameters are directly retrieved for ascending (positive parameters indexed by a plus) and descending (negative parameters indexed by a minus) ejecta crossing the successive range gates above, or on either side of, the eruptive jet axis: (1) velocity information, in particular maximum and mean radial velocity (V^+_{max}, V^-_{max}, V^+_{mean}, V^-_{mean}) and (2) power (P_+, P_-) backscattered by particles contained in the sampling volume at a given instant [*Dubosclard et al.*, 2004].

[9] The received echo power from the particles (spectral moment of order 0) can be defined by the integral of the spectral power density $S(v)$ in a velocity interval between

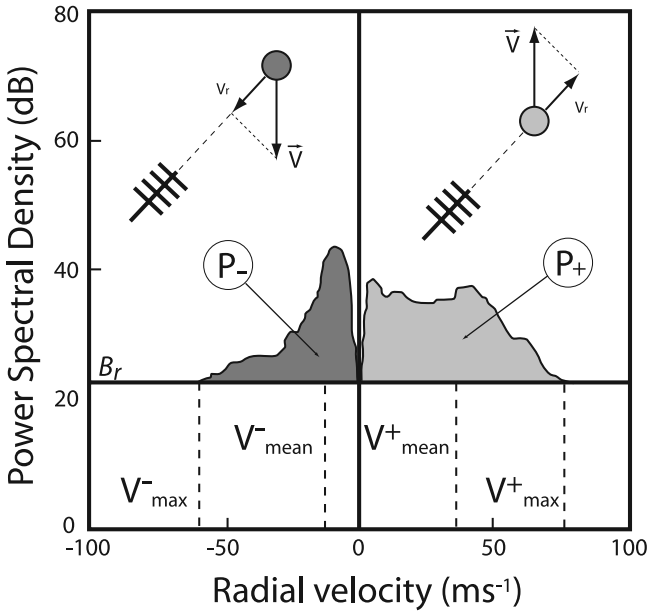

Figure 2. Sketch of a typical Doppler spectrum obtained by VOLDORAD. The power spectral density is displayed as a function of the radial velocity in a given range. The horizontal line (B_r) corresponds to the background noise level. Total echo power and maximum and mean velocities can be deduced from Doppler spectra. They are indexed (plus) and (minus) for ejecta with the radial component of their velocity vector moving away and toward the antenna, respectively.

Table 2. Gate Center Coordinates[a]

	G_1	G_2	G_3	G_4
Gate angle to the vertical (deg)	78	34	−23	−43
Slanting distance to the radar (m)	807	927	1047	1167
Horizontal distance to the crater (m)	−166	−56	54	165
Elevation above crater rim (m)	33	80	127	174
Gate height (m)	127	146	165	184

[a] G_1 to G_4, for an elevation angle of 23° and pulse duration of 0.8 μs.

v and $v + dv$, from 0 to $V^+_{\max}$ for ascending particles and from $V^-_{\max}$ to 0 for descending particles. The power measured in the Doppler spectra has been calibrated in the laboratory by means of an input signal, the power of which was known, delivered by an external frequency generator:

$$P_+ = \int_0^{V^+_{\max}} S(v)dv, \quad P_- = \int_{V^-_{\max}}^0 S(v)dv \tag{4}$$

Maximum radial velocities in the directions toward and opposite to the radar, $V^-_{\max}$ and $V^+_{\max}$, respectively, are defined where $S(v)$ is equal to the background noise level B_r (Figure 2). Likewise, for a given Doppler spectrum, V^+_{mean} and V^-_{mean} (spectral moment of order 1) of the ejecta are given by

$$V^+_{\text{mean}} = \frac{\int_0^{V^+_{\max}} vS(v)dv}{\int_0^{V^+_{\max}} S(v)dv}, \quad V^-_{\text{mean}} = \frac{\int_{V^-_{\max}}^0 vS(v)dv}{\int_{V^-_{\max}}^0 S(v)dv} \tag{5}$$

3. Electromagnetic Scattering Model

[10] The aim of this study is to estimate masses of volcanic ejecta from two Strombolian explosions with contrasted particle loads by inversion of the Doppler radar measurements. For this purpose, a comparison between the backscattered power measured by the radar (P_{mes}) and the synthetic (i.e., calculated) backscattered power (P_{synth}) is needed (see section 4. for more details on the inversion method). In this section, we first describe how to retrieve P_{mes}, and then we derive P_{synth} using the electromagnetic scattering theory of *Mie* [1908]. As shown by Figure 2, processing of the Doppler spectra yields the total backscattered power ($P_{\text{tot}} = P_- + P_+$). Raw power values ($P_{\text{mes}}$) can then be deduced directly from the radar conversion constant (C_c) that depends on technical characteristics of the radar acquisition line:

$$P_{\text{mes}} = P_{\text{tot}} C_c \tag{6}$$

On the other hand, P_{synth} can be derived from an electromagnetic scattering model. A good approximation for small particles is the Rayleigh scattering theory, the validity limit of which depends on the radar wavelength [*Sauvageot*, 1992]. This method is commonly used in meteorology, because the typical diameter of water droplets is small compared to the wavelengths of meteorological radars. In our case (λ = 23.5 cm), the Rayleigh theory can only be applied for particles of diameter (D_L) smaller than $\lambda/4$, which corresponds to ~5.9 cm [*Gouhier and Donnadieu*, 2006]. However, considering the wide range of particle diameters characterizing volcanic activity, the complete scattering theory is required to account for the effects of larger particles. A general solution of electromagnetic wave scattering was given by *Mie* [1908]. This approach applies Maxwell's equations for plane waves scattered by compositionally homogeneous particles (Appendix A). For application to volcanic eruptions, we focus on waves scattered at a large distance by spherical particles, which we assume are homogeneously distributed in space. Theoretically, the power backscattered to the radar by a population of such particles in a given range gate is proportional to their radar reflectivity (η). The synthetic power can then be defined as

$$P_{\text{synth}} = \frac{C_r V_s \eta}{R^4} \tag{7}$$

where C_r is the radar constant, V_s, the sampling volume, and R, the slant distance between the radar and the target. The radar constant is defined by a set of technical parameters related to the radar configuration. The radar constant has been calibrated using a classical method comparing the reflectivity of rainfalls probed by the radar and the reflectivity calculated from the drop size distribution and velocity of the falling hydrometeors measured simultaneously with a disdrometer [*Pointin et al.*, 2005]. The radar reflectivity (η) is the sum of the backscattering cross sections (σ_{bks}) of the individual particles per unit volume. The reflectivity factor (Z) is defined by *Sauvageot* [1992] as

$$\eta = \sum_{i=1}^{n} \frac{\sigma_{\text{bks}_{(i)}}}{V_s} \tag{8}$$

and

$$Z = \frac{\eta \lambda^4}{\pi^5 |K|^2} 10^{18} \tag{9}$$

Z (commonly confused with η in the literature) is often expressed in logarithmic units as dBZ and is related to η through the radar wavelength λ, and the particle complex dielectric factor $K = (m^2 - 1)/(m^2 + 2)$. Scattering and attenuation by compositionally homogeneous spheres are significantly influenced by the complex refractive index (m). VOLDORAD transmits power through a square array of four Yagi antennas, such that the incident electromagnetic wave is polarized parallel to the scattering plane. Being a monostatic radar (i.e., the same antenna is used for transmission and reception), we define a backscattering cross section (σ_{bks}) for horizontal linear polarization:

$$\sigma_{\text{bks}} = \frac{\lambda^2}{4\pi} \left| \sum_{n=1}^{\infty} (-1)^2 (2n+1)(a_n - b_n) \right|^2 \tag{10}$$

where a_n and b_n are the complex scattering coefficients (so-called Mie coefficients). Examples of Mie versus Rayleigh scattering patterns of an electromagnetic wave scattered by homogeneous spheres of four different sizes are shown in Figure 3 for a signal at the wavelength used by

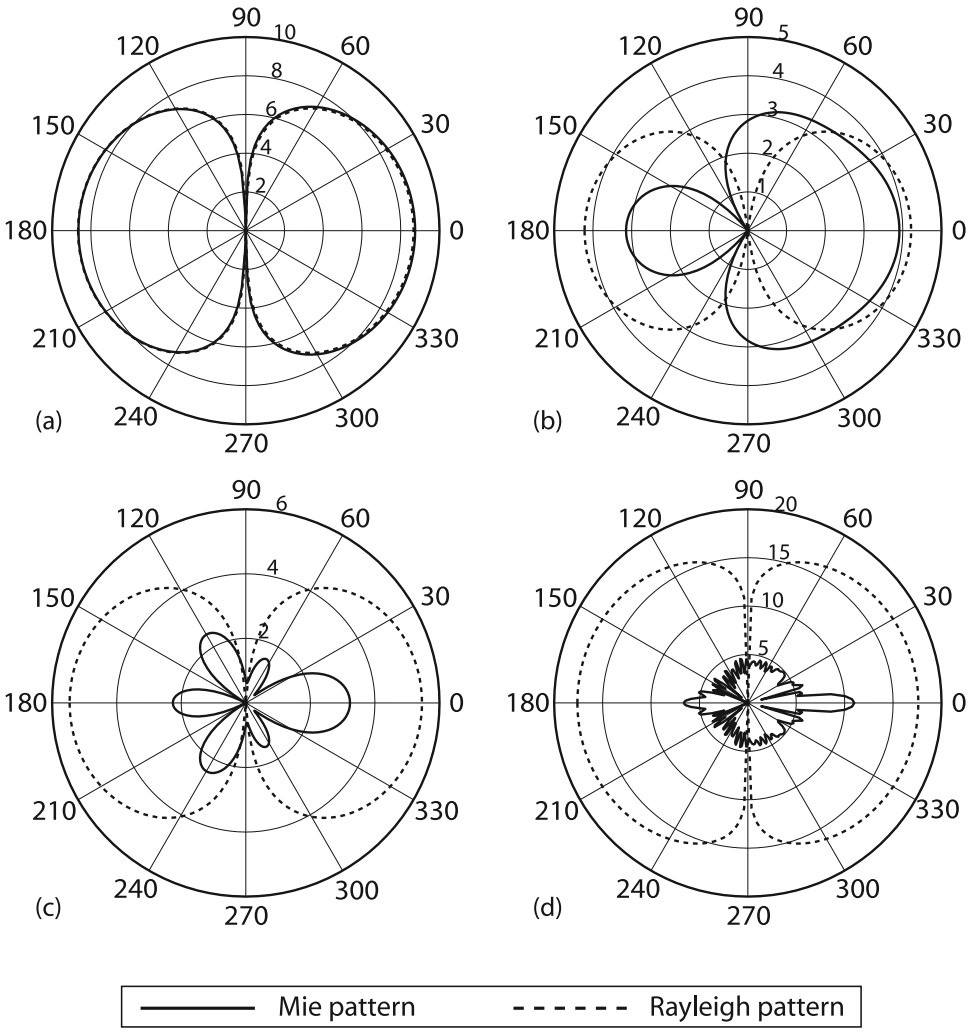

Figure 3. Mie versus Rayleigh scattering patterns of an electromagnetic wave, parallel polarized, scattered by a single homogeneous sphere with the complex dielectric factor of volcanic ash, $|K|^2 = 0.39$ [*Adams et al.*, 1996], and $\lambda = 23.5$ cm. The wave arrives from the left, and the particle is situated at the center of the pattern. Irradiance amplitude is normalized to that of Mie and expressed on a logarithmic scale. (a) Example of a small particle of diameter 2 cm. The Rayleigh and Mie scattering patterns are identical and symmetrical. Irradiance intensity is the same in front of and behind the particle. (b) Particle of diameter 14 cm. The Rayleigh and Mie scattering patterns are now significantly different. The Mie pattern still has two main lobes but is strongly asymmetric, as the backscattered intensity is lower than the forward scattered intensity. (c) Particle of diameter 20 cm. The Rayleigh pattern is still symmetrical, whereas the Mie pattern is divided into several lobes and shows much lower values of irradiance. (d) For a diameter of 2 m, the Mie (true) scattering pattern becomes very complex and shows always much lower values of irradiance than the Rayleigh approximation.

VOLDORAD ($\lambda = 23.5$ cm) and with the complex dielectric factor of volcanic ash ($|K|^2 = 0.39$) [*Adams et al.*, 1996]. These patterns illustrate the large discrepancy between the Rayleigh and Mie formulations for particle diameters larger than a few centimeters at 23.5 cm wavelength. Note that, at smaller radar wavelengths, this discrepancy occurs at even smaller particle diameters, making the complete Mie formulation absolutely necessary for studies of volcanic ejecta from radar measurements.

[11] Figure 4 shows the reflectivity factor (Z) as a function of particle diameter, using both the Mie and Rayleigh formulations for a wavelength of 23.5 cm. Note the overestimation of Z when computed using the Rayleigh approximation for particle diameters greater than ~5.9 cm.

4. Inversion Method

[12] Model inversions are frequently used in geophysics to recover initial parameters and boundary conditions from observed data of natural phenomena. In this case, backscattered power values (P_{mes}) are retrieved from radar measurements, and synthetic power data (P_{synth}) are determined from the forward electromagnetic-scattering model. The inversion algorithm thus seeks the best correlation between P_{mes} and P_{synth}, providing the optimum variable

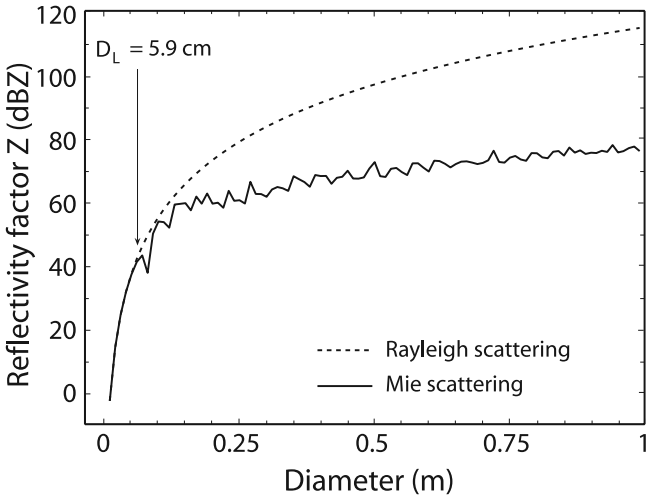

Figure 4. Synthetic reflectivity factor (Z, expressed in dBZ) as a function of particle diameter. Note the large overestimation of Z for large diameters when computed using the Rayleigh approximation. The validity domain depends on the radar wavelength. In the case of VOLDORAD (λ = 23.5 cm), the validity limit (D_L) lies close to 5.9 cm, i.e., $\sim\lambda/4$ [*Gouhier and Donnadieu*, 2006].

input parameters defined by the vector (X) that characterizes the PSD. Physical parameters such as particle mass and volume are then deduced from the PSD. The model takes into account two main classes of parameters: (1) constant parameters describing the geometry of the system, the technical characteristics of the radar or material physical properties; (2) the vector of variable input parameters (X; see below) defining the Weibull function of the PSD. A least squares estimation method is used on the basis of the minimization function $S(X)$ characterized by the squared residual between radar measured data and synthetic data:

$$S(X) = \sum \left[P_{\text{mes}} - P_{\text{synth}}(X)\right]^2 \tag{11}$$

Finally, a comparison criterion between radar-measured (P_{mes}) and synthetic (P_{synth}) power data is used to stop the recursive loop when the fitting criterion is reached. The successive steps of the inversion algorithm are summarized below.

[13] Step 0 is attribution of initial values for estimation of the input parameters:

$$X_j \equiv [X_1, X_2, \ldots, X_n]$$

[14] Step 1 is resolution of the direct model (Mie scattering):

$$X \rightarrow P(X)_{\text{synth}}$$

[15] Step 2 is calculation of the minimization function:

$$S(X) = \sum \left[P_{\text{mes}} - P_{\text{synth}}(X)\right]^2$$

[16] Step 3 is characterization of the iterative comparison criterion:

$$\Delta P(X^i) = S(X^{i-1}) - S(X^i)$$

[17] Step 4 is testing of the fitness criterion:

$$\Delta P(X) < 0$$

where $\Delta P(X)$ is the fitness criterion, and indices i and j refer to the step of the iterative procedure and the number of variable parameters, respectively. When a satisfactory solution is reached, the iterative procedure stops. The computational procedure is summarized in Figure 5.

5. Polydisperse Particle Size Model

5.1. Particle Size Distribution

[18] Solving the inverse problem consists of estimating the shape of the PSD by best fit matching of synthetic and observed data. Various PSDs have been used in, or inferred from, previous studies of volcanic ejecta: exponential [*Ripepe et al.*, 1993], lognormal [*Sheridan*, 1971; *Chouet et al.*, 1974; *McGetchin et al.*, 1974; *Self et al.*, 1974], Rosin

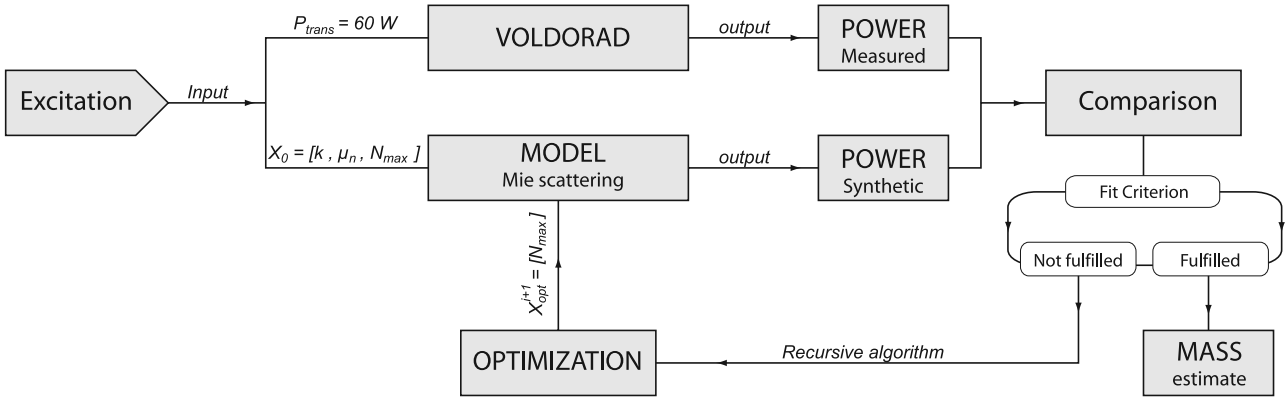

Figure 5. Sketch of the inversion approach. Synthetic radar power data (P_{synth}) are provided from the theoretical model (Mie formulation) and compared to the power data measured (P_{mes}) by VOLDORAD. If the fit criterion is met, the procedure stops and gives the best result. Otherwise, the input parameters (X) are optimized in the recursive loop, and the calculation is repeated.

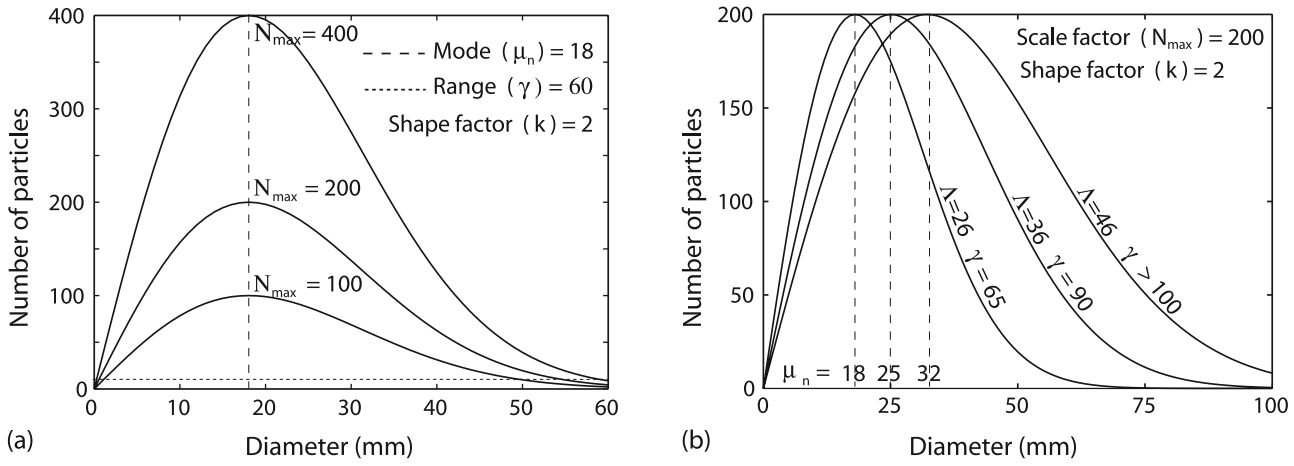

Figure 6. Evolution of the particle size distribution (PSD) for different values of shift (Λ) and scale factors ($N_{\max}$). For both examples, the shape factor is constant at $k = 2$. (a) The scale factor ($N_{\max}$) represents the maximum number of particles with diameter μ_n and, therefore, directly controls the total number of particles. (b) The mode (μ_n) and range (γ) of the distribution evolve jointly with the shift factor.

Rammler [*Kittleman*, 1964; *Spieler et al.*, 2003], Weibull [*Nakamura*, 1984; *Marzano et al.*, 2006a, 2006b], polymodal [*Sheridan et al.*, 1987; *Riley et al.*, 2003] and sequential fragmentation/transport (SFT) [*Wohletz et al.*, 1989]. However, there is still a lack of consensus on which PSD best characterizes Strombolian activity, particularly for the largest particle diameters. For this reason, a scaled Weibull function is used, because its overall shape may be varied widely from exponential to Gaussian by means of only three factors: shape (k), shift (Λ), and scale ($N_{\max}$). The PSD can then be adjusted easily during the optimization phase of the data inversion procedure. The scaled Weibull distribution S_w is defined through a probability density function f_w of particles with diameter D:

$$S_w(D;k,\Lambda,N_{\max}) = \frac{f_w(D;k,\Lambda)}{\max[f_w(D;k,\Lambda)]} N_{\max} \tag{12}$$

with

$$f_w(D;k,\Lambda) = \left(\frac{k}{\Lambda}\right)\left(\frac{D}{\Lambda}\right)^{(k-1)} \exp\left(\frac{-D}{\Lambda}\right)^{k} \tag{13}$$

The shape factor (k) allows us to choose from an exponential ($k = 1$) to Gaussian ($k = 3$) distribution, along with all intermediate lognormal distributions ($1 < k < 3$). The shift factor (Λ) directly depends on the mode (μ_n) of the PSD and on the shape factor (k). It can be defined by using

$$\Lambda = \mu_n \left(\frac{k-1}{k}\right)^{-1/k} \tag{14}$$

$N_{\max}$ is the maximum number of particles of diameter μ_n in the scaled Weibull distribution (Figure 6a). It is the dominant term in the computation of the synthetic power because it strongly influences the estimate of particle mass.

[19] The three variable parameters (k, μ_n, $N_{\max}$) controlling the PSD make up the vector X of input parameters to the model. However, in order to obtain a unique solution to the inverse problem, the number of variable parameters is reduced. This also increases the efficiency and speed of the algorithm. Parameters k and μ_n are constrained from the following assumptions argued in subsequent sections: (1) the PSD of Strombolian explosions can be characterized on average by a single shape factor k; (2) the mode of the PSD (μ_n) can be determined from mean particle terminal velocity estimated from the radar measurements. These assumptions then reduce the optimization procedure to a single free parameter ($N_{\max}$).

5.2. Parameter Constraints

5.2.1. Shape Factor, *k*

[20] Data on Strombolian PSDs are scarce in the literature. However, *Chouet et al.* [1974] gave an exhaustive description of two explosions at Stromboli Volcano by photoballistic analysis. They made an estimate of the PSD for inflight ejecta (which is what a radar records), and determined the modes, ranges, numbers and sizes of particles for two explosions. They also deduced eruptive parameters such as number, mass and volume of ejected particles, and found that one explosion contained a number and mass of particles about 17 times greater than the other (Table 3). We use this study, where all output parameters are already known, to determine the input parameter (k) that best describes the two Strombolian explosions observed by *Chouet et al.* [1974]. With this aim, we first calculate the "equivalent" radar power corresponding to the total ejected mass estimated by *Chouet et al.*'s [1974] observations for two Strombolian explosions. Then synthetic radar powers are computed for different values of shape factor k. Finally, the recursive procedure stops when synthetic radar powers match the equivalent radar power and when synthetic particle loading parameters (number, mass, volume) corre-

Table 3. Comparison Between Values Observed by *Chouet et al.* [1974] on Two Explosions at Stromboli and Synthetic Values Calculated by the Inversion Algorithm[a]

		Explosion 1: Sep 1971		Explosion 2: Sep 1971	
	Symbol	Observed Data	Synthetic Data	Observed Data	Synthetic Data
Number of particles	N	2588	2588	146	144
Mode (m)	μ_n	0.022	0.022	0.025	0.025
Range (m)	γ	?–0.06	0.004–0.06	?–0.06	0.001–0.06
Volume (m^3)	V	0.033	0.035	0.002	0.0027
Mass (kg)	M	51	53	3	4.1

[a]Note that the best fit for both sets of data is reached for the same shape factor $k = 2.3$ (lognormal particle size distribution).

spond to those described by *Chouet et al.* [1974]. Note that an alternative method would have been simply to determine k from a best fit function of the *Chouet et al.* [1974] PSD. However, our chosen approach had the advantage of additionally testing our inversion algorithm.

[21] The best fit between the observed and synthetic PSDs is reached in both cases for the same value of $k = 2.3$, which describes a lognormal distribution. The equivalent synthetic power achieved is about 3.3×10^{-9} and 3.2×10^{-10} mW for explosions 1 and 2 respectively, and corresponds to equivalent reflectivity factors (Z) of 61 and 51 dBZ. The inversion procedure yields three parameters (number, mode and range) characterizing the synthetic PSDs, from which two eruptive parameters (mass and volume) are directly deduced (Table 3). The agreement between observed and synthetic parameters is very good and validates our inversion algorithm. Shape factor estimation can then be used afterward with reasonable confidence. Furthermore lognormal PSDs have also been inferred from deposits of Strombolian activity on other volcanoes, like Etna [*McGetchin et al.*, 1974] and Heimaey [*Self et al.*, 1974]. Although k may vary between individual explosions on Stromboli, as well as between Strombolian eruptions at different volcanoes, we assume in what follows that the value $k = 2.3$, found for both explosions at Stromboli, represents a suitable average value for Strombolian PSDs and use it as input to the model. Moreover, sensitivity tests reveal a limited dependence of the total ejected mass on k, varying only by a factor of two for values of k ranging from 2.0 to 2.6.

5.2.2. Shift Factor, Λ

[22] The shift factor (Λ) is linked to the mode (μ_n) and range (γ) via the shape factor (k) (Figure 6b). The mode of the distribution is estimated directly from radar measurements using the terminal settling velocities of ejected particles. Indeed, under the assumptions of vertical trajectories, no wind influence, and terminal fall velocity, an average particle diameter D_p can be deduced from the mean negative radial velocity weighted by the power spectral density [*Rogers and Yau*, 1989; *Hort et al.*, 2003]

$$D_p = \frac{C_s}{P_-} \sum_{V_{\max}^-}^{0} S(v) \left(\frac{V_r}{\sin\theta} \right)^2 \tag{15}$$

where $S(v)$ is the spectral power in a velocity interval. P_- refers to the power backscattered mainly by descending particles (left part of the Doppler spectrum), and θ stands for the antenna beam elevation angle. C_s is the shape coefficient, which for a spherical particle is:

$$C_s = \frac{3}{4} C_d \frac{\rho_a}{\rho_p g} \tag{16}$$

with C_d being the drag coefficient, g the gravitational acceleration and ρ_a, ρ_p the densities of air and particles respectively. Importantly, the interpretation of D_p retrieved from Doppler radar spectra differs significantly from μ_n (the mode of the PSD). Indeed, μ_n corresponds to the particle diameter that is most represented in the particle size distribution, i.e., the top of the curve. In radar meteorology, D_p is approximately equal to μ_n because the size distributions of atmospheric water droplets are typically Gaussian and very narrow. In a volcanic jet however, the power spectrum is much wider [e.g., *Dubosclard et al.*, 1999], and the physical interpretation of D_p is therefore more complex. D_p and μ_n are offset by a factor based on the dependence of the reflectivity (calculated at a given radar wavelength) on the number (N) and diameter (D) of particles. Thus μ_n is obtained from D_p using a scattering formulation adequate for the range of particle sizes characterizing explosive volcanic activity [*Woods and Bursik*, 1991; *Gouhier and Donnadieu*, 2006]. Once k and μ_n are obtained, the shift factor Λ can be calculated from equation (14).

5.2.3. Scale Factor, $N_{\max}$

[23] By assuming that k and μ_n are constant throughout the inversion procedure, the parameter vector X then becomes dependent on just a single free parameter, the scale factor, $N_{\max}$. This characterizes the maximum of the scaled Weibull distribution curve (S_w) and evolves during the optimization phase of the algorithm. It describes, along with k and μ_n, the total number of particles ejected during the explosion, and hence controls the erupted mass estimation. The accuracy of the results depends on the step chosen between two successive values of $N_{\max}$ in the recursive loop. However, although a small step leads to a more accurate estimation, it increases considerably the computing time.

6. Monodisperse Particle Size Model

[24] An alternative data inversion model based on a monodisperse PSD approximation is now presented. In this model, the single particle size equals μ_n, as well as D_p.

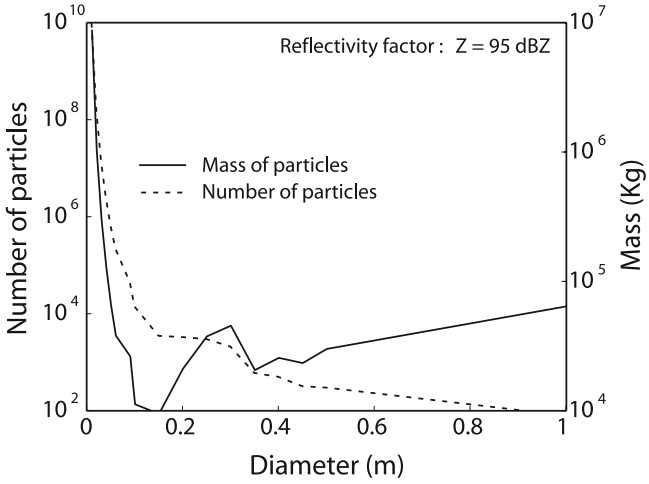

Figure 7. Plot of the total mass and number of particles as a function of their diameter in the monodisperse model for a reflectivity factor $Z = 95$ dBZ. Small particles contribute the most to the total ejected mass, for example, 8.8×10^6 kg for a diameter of 0.01 m, compared to 6.4×10^4 kg for a diameter of 1 m, i.e., a difference of 2 orders of magnitude.

Figure 7 shows that the number of small particles required to generate a given reflectivity can be up to several orders of magnitude larger than the number of corresponding large particles. Because of this huge difference in particle number, the fraction of small ejecta contributes most to the total estimated mass. For example, a reflectivity of 95 dBZ requires 8.8×10^6 kg of 0.01 m particles compared to 6.4×10^4 kg of 1 m particles, a difference of 2 orders of magnitude. This result illustrates that large blocks are not so important in first-order estimations of total ejected mass.

This monodisperse PSD model significantly reduces computing time and ensures fast synthetic power calculations. Mass estimations are provided in Figure 8 for a wide range of realistic values of D_p and Z. Since these parameters are derived directly from the Doppler spectra, the corresponding mass can be retrieved instantaneously without any computing phase. This alternative method is valuable because a first-order mass estimate of ejected pyroclasts can be obtained in real time and used for volcano monitoring.

7. Radar Data

[25] Strombolian explosions and lava fountains were monitored with VOLDORAD for several hours during eruptive episodes of the SE crater on 4, 7, and 13 July 2001. We focus on data acquired during two explosions that occurred at 2141:53 and 2141:56 UT during the eruption of 4 July. The two explosions were each short-lived, with durations of about 3 s. Temporal series (Figure 9) of radar power are computed from the power spectral density $S(v)$, and sampled at a high frequency (10 Hz) suitable for such short-lived explosions.

[26] It is important that the power used as input to the inversion model be defined carefully. First, it is essential to ensure that the total power at a given instant is the sum of P_{tot} across the different range gates along the beam axis. Were the jet wider than the width of a single range gate (120 m), it would be necessary to integrate across several range gates in order to obtain the total reflected power. However, in the cases studied here, both jets were sufficiently narrow as to fit within a single range gate (G_3). This is deduced from (1) visual inspection of video snapshots and (2) the lack of echo power signal from neighboring range

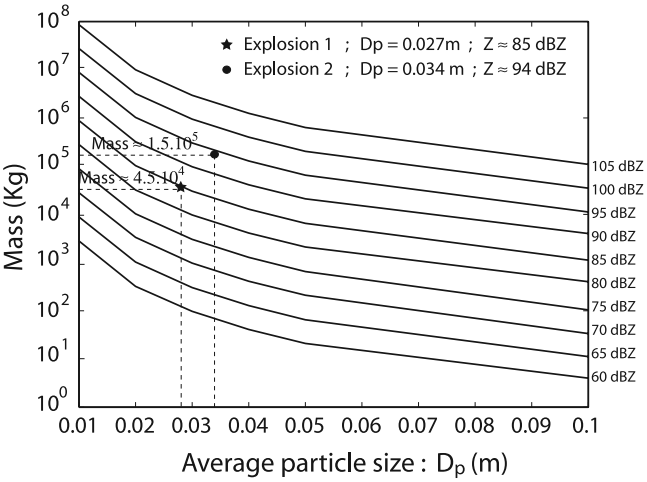

Figure 8. Mass estimate as a function of average particle size (D_p) retrieved from the power spectral density using the monodisperse model for different reflectivity factors (Z) of ejected particles. First-order mass assessments can be given simply from the reflectivity factor (Z) and the average particle size (D_p) determined directly from the Doppler spectra, without any computation phase. Masses of 4.5×10^4 kg and 1.5×10^5 kg are roughly estimated for explosions 1 and 2, respectively.

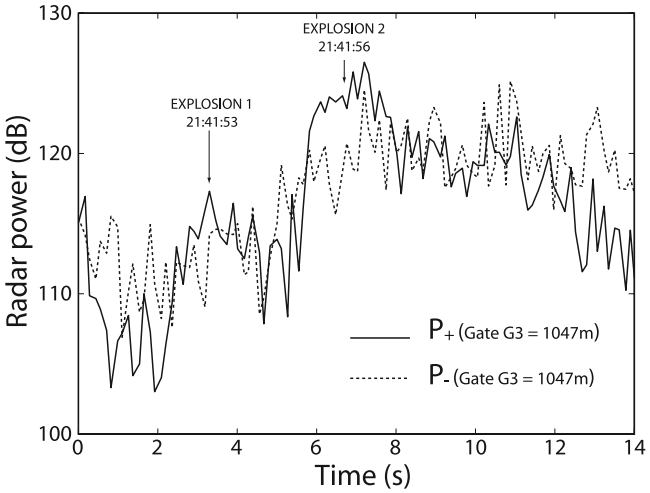

Figure 9. Temporal evolution of radar echo power during the two explosions studied at Mount Etna on 4 July 2001, sampled at 10 Hz. Both echo powers of particles moving away from (P_+) and toward (P_-) the antenna are plotted in order to infer the total power at a given instant in the range gate (G_3) located above the vent. Both explosions are brief, lasting 2.2 and 2.8 s, respectively. The second explosion is much more powerful (125 and 123 dB for P_+ and P_-, respectively) than the first (117 and 115 dB).

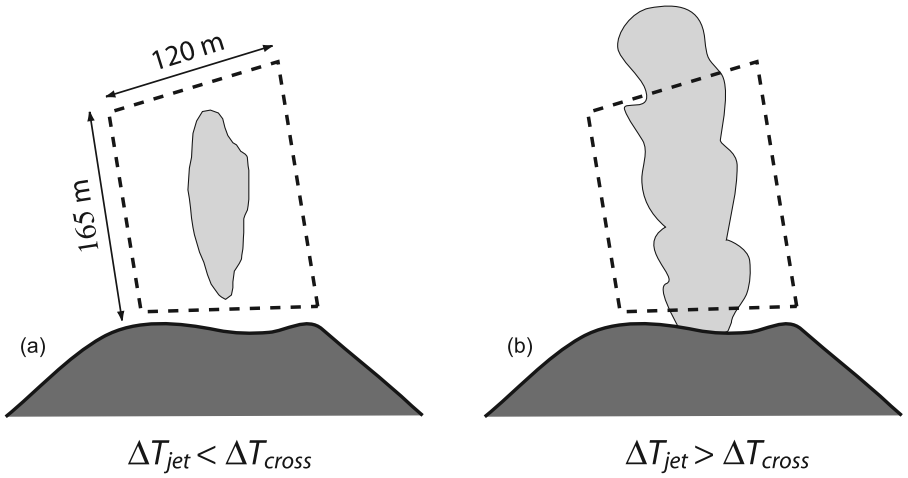

Figure 10. Sketch illustrating the two hypotheses made in the calculation of total power. Δt_{jet} is the duration of jet production, and Δt_{cross} is the time necessary for the jet to traverse vertically the range gate. (a) Example of a short-lived jet ($\Delta t_{jet} < \Delta t_{cross}$): the jet is short enough to be wholly enclosed in the sampling volume. A single Doppler spectrum can then be used for the calculation of total power. (b) Example of a long-lived jet ($\Delta t_{jet} > \Delta t_{cross}$): the jet is too long to be contained entirely in the sample volume at a given instant. The maximum radar echo power represents only a fraction of the total amount of ejected particles, and several Doppler spectra have to be taken into account for the calculation of the total power. The two explosions jets of 4 July 2001 at Mount Etna studied in this paper were both short-lived.

gates (G_2 and G_4). Integration along the beam axis is therefore unnecessary.

[27] The second requirement is that the reflected power be integrated throughout the entire duration of the explosion as the jet passes vertically across the range gate concerned (G_3). In this case, two situations can be envisaged, as shown schematically in Figure 10. To explain these two cases, we consider two time durations: Δt_{jet}, the duration of jet production, and Δt_{cross}, the time necessary for the jet to traverse vertically the given range gate. In the first case (Figure 10a), $\Delta t_{jet} < \Delta t_{cross}$ and the jet is thus short enough for most of the particles to be recorded at the same instant inside a single sampling volume. The peak of radar echo power can therefore be considered as representative of the entire jet and the input parameters to the model can be derived on the basis of a single Doppler spectrum. When $\Delta t_{jet} \geq \Delta t_{cross}$ (Figure 10b), the jet is never entirely contained within a single range gate, and the peak of echo power represents only a fraction of the constituent particles. Integration over the duration of the jet (Δt_{jet}) is therefore essential. Note that for lava fountaining sustained over longer periods of time at a relatively steady rate, the mean residence time of ejecta inside the range gate would need to be taken into account. This could be inferred from velocities measured by the radar and from the sounding geometry, leading to estimation of the mass flux. The total mass of lava ejected could then be calculated using the duration of the lava fountain.

[28] In the explosions considered here, the average time Δt_{cross} taken by the jet to cross the range gate (G_3) is 4.7 s at an average velocity of 38 m s^{-1} for explosion 1, and 2.9 s at 62 m s^{-1} for explosion 2. By comparison, Δt_{jet} is estimated from videos and radar time series at 2.2 and 2.8 s for explosions 1 and 2, respectively. In both cases, therefore, $\Delta t_{jet} < \Delta t_{cross}$; no time integration is necessary, and data analysis can be based on a single Doppler spectrum. Moreover, the explosion jets commonly become depleted in blocks, and proportionally richer in gas toward the waning stage of their emission, so that the relevant values for Δt_{jet} might actually even be lower.

8. Results

[29] Results of the polydisperse and monodisperse models are shown in Tables 4a–4c and 5a–5c. The fitness between observed and synthetic power data is very good, with 98.7% and 97.8% for explosions 1 and 2, respectively.

8.1. Particle Loading Parameters

[30] Using the more accurate polydisperse model, the total mass of pyroclasts ejected by the first explosion (Tables 4a–4c) is estimated at 58,400 kg, corresponding

Table 4a. Synthetic Results for Explosion 1 (2141:53 UT) at Mount Etna SE Crater[a]

		Synthetic Results	
	Symbol	Monodisperse PSD	Polydisperse PSD
Number of particles	N	2.75×10^6	13.9×10^6
Mode (m)	μ_n	0.027	0.013
Volume (m^3)	V	28.4	38.2
Mass (kg)	M	43.4×10^3	58.4×10^3
Concentration[b] (kg m^{-3})	C	0.01–0.2	0.02–0.4
Reflectivity factor (dBZ)	Z	85.16	85.13
Power (mW)	P_{synth}	8.14×10^{-7}	8.08×10^{-7}

[a]Results are from using both the polydisperse particle size distribution model and the monodisperse approximation.

[b]Concentration parameters are poorly constrained and have to be regarded as rough approximations (see text for details).

Table 4b. Model Parameters for Explosion 1 (2141:53 UT) at Mount Etna SE Crater

Parameters	Input/Output
μ_n	0.0129
D_p	0.027
Λ	0.0165
k	2.3
γ	0.01–0.056
N_{max}	8.00×10^5
Fit (%)	98.68

to a volume of 38 m^3 assuming a pyroclast density of 1530 kg m^{-3} [*McGetchin et al.*, 1974] and a reflectivity factor of 85 dB*Z*. The equivalent magma volume (DRE), for a density of 2700 kg m^{-3} [*Williams and McBirney*, 1979] is 22 m^3. The second explosion (Tables 5a–5c) yields higher values of the different parameters, with an ejecta mass of 206,000 kg, a pyroclast volume of 135 m^3, a reflectivity factor of 94 dB*Z*, and a magma volume of 76 m^3. The difference between the reflectivity factors of the two explosions is 9 dB*Z*, meaning that the second explosion jet is about 8 times more reflective than the first, and the ejecta volume and mass are consequently about 3.5 times higher. This agrees with visual observations which show clearly that the first explosion involved a smaller quantity of incandescent lava clots than the second explosion (Figure 11).

[31] Particles numbers, masses and volumes estimated using the monodisperse model lie within ~25% of those of the polydisperse model for both explosions (Tables 4a–4c and 5a–5c). This underestimation is accounted for by small particles that are not considered in the monodisperse model, but that in reality contribute most to the total mass, owing to the great particle number required to match a given reflectivity.

[32] It is instructive to compare the measured reflectivity factors of the two Etna explosions with those theoretically calculated at Stromboli from the *Chouet et al.* [1974] observations. Recall that reflectivity factor (*Z*) is a positive function of the number (*N*) and diameters (*D*) of ejected particles. The two explosions at Stromboli give reflectivity factors of 61 dB*Z* and 51 dB*Z* (Table 3), whereas the two explosions at Etna give 85 and 94 dB*Z* (Tables 4a–4c and 5a–5c). Thus, even a small explosion at Etna is over 250 times more reflective than a large one at Stromboli, and involves a mass of ejecta 3 orders of magnitude higher (Table 3). For comparison, very heavy rainfall induces maximum reflectivity factors of ~60 dB*Z* [*Sauvageot*, 1992].

Table 4c. Characteristics for Explosion 1 (2141:53 UT) at Mount Etna SE Crater

Characteristic	Value
Date	4 July 2001
Time (UT)	2141:53
t_{jet} (s)	2.2
$\bar{V}^+_{max}$ (m/s)	60
$\bar{V}^{+\,a}_{max}$ (m/s)	37.9
Z (dBZ)	85.12
P_{mes} (mW)	8.10×10^{-7}

[a]The parameter $\bar{V}^+_{max}$ is the time-averaged maximum velocity and differs from the mean velocity calculated by the radar.

Table 5a. Synthetic Results for Explosion 2 (2141:56 UT) at Mount Etna SE Crater[a]

		Synthetic Results	
	Symbol	Monodisperse PSD	Polydisperse PSD
Number of particles	N	5.00×10^6	23.3×10^6
Mode (m)	μ_n	0.034	0.016
Volume (m^3)	V	102.9	134.7
Mass (kg)	M	157×10^3	206×10^3
Concentration[b] (kg m^{-3})	C	0.05–0.1	0.06–0.12
Reflectivity factor (dBZ)	Z	93.78	93.77
Power (mW)	P_{synth}	5.92×10^{-6}	5.87×10^{-6}

[a]Results are from using both the polydisperse particle size distribution model and the monodisperse approximation.

[b]Concentration parameters are poorly constrained and have to be regarded as rough approximations (see text for details).

8.2. Derived Parameters

[33] The mean mass fluxes of ejecta, estimated from the duration of each explosion (Tables 4a–4c and 5a–5c), reach 26,400 and 73,600 kg s^{-1} for explosions 1 and 2, respectively. These represent time-averaged values, and are not expected to be constant over the duration of each explosion.

[34] We have also attempted to estimate particle concentrations in the two explosion jets at Etna. This is difficult since, although the radar data provide estimates of total particle mass, the jet volumes are poorly constrained. One possibility is to make the assumption that each jet filled completely and homogeneously the range gate volume. In this case, concentration estimates have to be regarded as minima. Using the volume of range gate (G_3) above the crater yields values of 0.02 and 0.06 kg m^{-3} for explosions 1 and 2, respectively. However, inspection of video footage (Figure 11) shows that this assumption is probably not realistic. The other option is to make an estimate of the jet volume from video snapshot analysis, but two difficulties are inherent in this approach: first, the jets are spatially heterogeneous, and, second, only large lava clots are visible and the volume occupied by ash and small laplli cannot be estimated. However, taking limiting edges on video snapshots yields that the jets of explosions 1 and 2 represent approximately 5% and 50%, respectively, of the range gate volume. Using these values gives maximum particle concentrations estimates of about 0.4 and 0.12 kg m^{-3} for explosion jets 1 and 2, respectively (Tables 4a–4c and 5a–5c). Note that these concentrations represent spatially averaged values over the estimated jet volume; however, much higher ejecta concentrations can be found locally especially close to the vent.

[35] The high data sampling rate (~10 Hz in the configuration used for this study) allows VOLDORAD to measure rapid signal fluctuations on the timescale of an individual

Table 5b. Model Parameters for Explosion 1 (2141:56 UT) at Mount Etna SE Crater

Parameters	Input/Output
μ_n	0.0164
D_p	0.034
Λ	0.021
k	2.3
γ	0.01–0.072
N_{max}	1.05×10^6
Fit (%)	97.82

Table 5c. Characteristics for Explosion 2 (2141:56 UT) at Mount Etna SE Crater

Characteristic	Value
Date	4 July 2001
Time (UT)	2141:56
t_{jet} (s)	2.8
$\bar{V}^{+}_{max}$ (m/s)	100
$\bar{V}^{+}_{max}$ [a](m/s)	61.6
Z (dBZ)	93.83
P_{mes} (mW)	6.00×10^{-6}

[a]The parameter $\bar{V}^{+}_{max}$ is the time-averaged maximum velocity and differs from the mean velocity calculated by the radar.

explosion. It is therefore possible to calculate an average ejecta velocity, and hence a mean kinetic energy for an explosion, using

$$E_k = \frac{1}{2} M \left(\frac{1}{N_t} \sum_{i=1}^{n} V^{+}_{max}(i) \right)^2 \quad (17)$$

where M is the total ejected mass given in Tables 4a and 5a and $\bar{V}^{+}_{max}$ is the maximum radial velocity, given in Tables 4c and 5c Doppler spectrum (i) recorded in the sampling volume. N_t is the total number of Doppler spectra acquired during a given explosion. A mean kinetic energy of 4.2×10^7 J is obtained for a time-averaged maximum radial velocity ($\bar{V}^{+}_{max}$) of 38 m s^{-1} for explosion 1 and 3.9×10^8 J for 62 m s^{-1} for explosion 2. These values can be compared with the thermal energies of explosions 1 and 2 from equation (18), which are estimated at 8.4×10^{10} J and 3×10^{11} J, respectively, assuming a magma temperature T of 1373 K [*Francalanci et al.*, 1989] and a magma specific heat capacity, C_p, of 1050 J kg^{-1} K^{-1} [*Vosteen and Schellschmidtb*, 2003]:

$$E_T = MTC_p \quad (18)$$

The thermal energies of the two explosions therefore exceed the kinetic energies by approximately 3 orders of magnitude. Note that the kinetic and thermal energies of the gas phase are not taken into account in these calculations.

8.3. Possible Effects of Outsized Particles

[36] The numerical approach to the inverse problem requires us to define a continuous theoretical function for the PSDs characterizing the explosions. In reality, however, explosion-generated PSDs might contain a coarse tail of large, discrete blocks which, although relatively small in number, could have a nonnegligible effect on the mass estimation. For example, the PSDs estimated photoballistically by *Chouet et al.* [1974] at Stromboli contained such coarse tails of blocks. Large blocks ejected during Strombolian explosions at Mount Etna have also been documented by *McGetchin et al.* [1974]. In the present study these have been neglected because they cannot be described by the type of continuous PSD function required by our automatized inversion algorithm. Manual runs have therefore been carried out to assess the sensitivity of mass calculations to an additional fraction of large particles. We define a composite PSD with a continuous part and an additional discrete part that constitute the lower and upper ranges, respectively, of the natural PSD (Figure 12). The coarse tail, consisting of 85 discrete blocks, is represented by an exponential distribution from 0.1 to 1 m in diameter with a median size of 0.23 m, i.e., close to that observed by

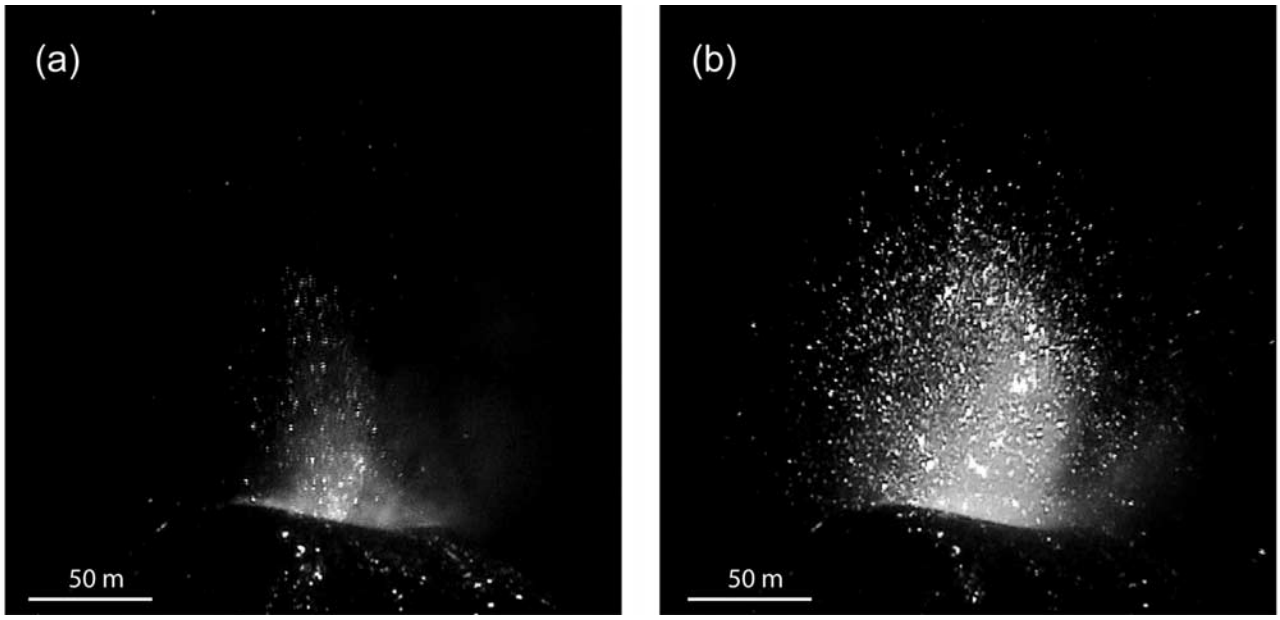

Figure 11. Snapshots of the two explosions from the SE crater of Mount Etna on 4 July 2001. Images are shown at maximum brightness, corresponding to the highest radar reflectivity from lava fragments. (a) The first explosion, occurring at 2141:53 UT, displays a low quantity of lava fragments and lasts 2.2 s, and (b) the second explosion, occurring at 2141:56 UT, displays a much higher number of lava fragments and lasts 2.8 s.

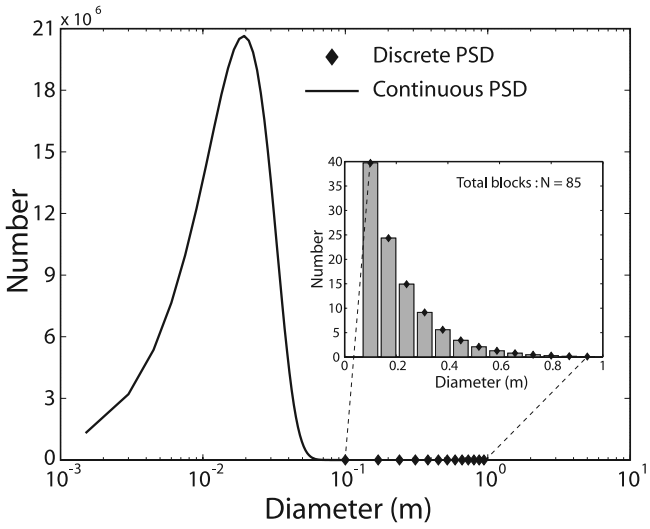

Figure 12. Composite particle size distribution comprising a continuous function to describe the smaller end of the PSD, with an additional coarse tail of large, discrete blocks. The continuous part refers to the PSD of explosion 2 calculated from our algorithm. The coarse tail is constrained from the data of *McGetchin et al.* [1974]; it consists of a total of only 85 blocks with a median size of 0.23 m, but that represents about 10% of the total reflectivity.

McGetchin et al. [1974] at the NE crater of Mount Etna (~0.2 m). Although numerically less abundant by more than 5 orders of magnitude than the smaller particles constituting the continuous PSD (Figure 12), the blocks of this coarse tail account for ~10% of the total reflectivity. This composite PSD is probably a more realistic representation of the explosion ejecta, and gives a total mass of 187,000 kg for explosion 2, in comparison to 206,000 kg for the continuous PSD lacking a coarse tail. We conclude that neglecting large blocks results in overestimation of the mass by only 9% for this explosion. This is because the total mass of pyroclasts is mostly controlled by the large number of small particles, as shown in Figure 7. As a result, all the mass-related parameters listed in Tables 4a–4c and 5a–5c can be regarded as maxima.

9. Discussion

[37] A Doppler radar (VOLDORAD) has been used to estimate for the first time a wide range of physical parameters characterizing Strombolian explosions at Mount Etna. In addition to the velocity data routinely provided by Doppler radar [*Donnadieu et al.*, 2005], the results yield estimates of particle loading (number, mass and volume), as well as derived parameters such as mass flux, time-averaged particle kinetic and thermal energies and, more approximately, particle concentration in the eruptive jet.

[38] Our approach in estimating particle loading, and the parameters derived from it, involves certain assumptions. For example, the electromagnetic scattering model assumes that all particles are smooth, spherical and compositionally homogeneous, which is not the case for pyroclasts. However, bearing in mind the statistical effects of a very large number of rough and complexly shaped particles, as well as our objective of first-order estimation, these simplifications seem reasonable. Another assumption concerns the particle size distribution (PSD) used for data inversion. The inversion procedure involves three physical parameters: two constants defining the PSD (mode and shape factor), and the third being the number of particles corresponding to the mode that evolves during the optimization phase of the inversion procedure. In the present study the mode was constrained from the radar measurements at Mount Etna. On the other hand, the shape factor was constrained independently using published photoballistic data of *Chouet et al.* [1974] from explosions at Stromboli, and was assumed to be representative of the explosion ejecta at Mount Etna. Many problems are inherent in this approach. For example, the photoballistically derived PSD of *Chouet et al.* [1974], while not skewed by atmospheric or depositional processes, is inadequate to describe the fine tail of the distribution, particles of which are too small to be detectable on photographs. On the other hand, *McGetchin et al.* [1974] constructed a PSD at Mount Etna from grain size measurements of Strombolian deposits, but this method also failed to take into account the smallest particles, which are dispersed far from source by the wind. Other difficulties involved in determining PSDs from deposits may also arise from bomb agglutination or from block breakage on impact. In addition, such studies probably fail to sample volumes of ejecta large enough to be statistically representative of real amounts of large blocks. Both photoballistic and ground deposits methods therefore fail to take into account small particles, whose contribution to the total mass is important. In contrast, UV satellite methods such as TOMS or more recently OMI [*Carn et al.*, 2008; *Krotkov et al.*, 2008], succeed in imaging gas (particularly SO2), ash and aerosols released by volcanic eruptions. The IR satellite methods such as Meteosat or MODIS [*Watson et al.*, 2004] are further able to provide estimates of the distal ash content of large eruptive clouds far from the emission source that are mainly composed of small particles. But these satellite-based methods fail to image the larger size fractions segregated earlier during plume ascent. These methods might also be biased by atmospheric effects on particles, such as water vapor content and ice formation. Nevertheless, the comparison of near-source estimates of ejecta mass from ground-based Doppler radar with the mass of distal fine ash estimated by satellite-based methods could bring valuable constraints on the particle segregation from ash clouds through space and time and hence on models of ash dispersal. In order to obtain more accurate values of the mass of ejecta, a more thorough knowledge must be acquired of total source granulometries of volcanic explosions, and of their variability for different eruptive regimes. Insights into such source PSDs could be gained for instance by high-resolution imagery and remote sensing methods working at different wavelengths. Such methods should target regions of the eruptive jet close to the vent in order for all ejected particles to be included. Their combination with ground ash collectors would bring even more stringent constraints. Knowledge acquired on PSDs would additionally provide further valuable insights into fragmentation and explosion processes during volcanic eruptions.

[39] By fixing the explosion source PSD shape factor independently, and by determining the PSD mode using the radar measurements, we obtain a way of estimating the particle loading parameters to a first approximation. Neglecting the inevitable coarse tail of large blocks appears justified on the basis of our calculations. The two PSD assumptions used in this paper each have different advantages. The polydisperse model requires an inversion procedure that takes a long time to compute, but which results in mass estimation to a reasonable first-order accuracy. This approach is probably best adapted to studies of eruption dynamics, where the most accurate possible parameter estimates are required. The monodisperse PSD model, on the other hand, does not require any computing phase, so that mass estimation is fast and straightforward. The disadvantage of this method is that it underestimates the particle loading. This monodisperse model is most suitable for volcano monitoring, where the eruptive parameters could be calculated automatically in real time from the Doppler spectra, but where a lower degree of accuracy could probably be tolerated.

[40] This study has shown that Doppler radar is a powerful, as yet underexploited, tool for quantitative studies of eruptive dynamics. The wide range of physical parameters accessible is potentially valuable for testing mathematical models of eruption jets and plumes. VOLDORAD is also well suited to the routine monitoring of active volcanoes. It can be sited at distances of up to 12 km from the vent, making it useful for the monitoring of large, highly explosive edifices. It functions under harsh weather conditions and has a data sampling rate suitable for the study of explosive activity. The relatively low energy consumption allows us either to set up the system quickly in the field with a small power generator for a limited period of time, or to run the radar continuously at a site supplied with electric power. In addition to classical continuous records of temporal series, VOLDORAD has a ''trigger'' mode, in which sequences of raw data can be recorded at high sampling rate, without basic processing and hence visualization. The system can be activated either on command of the operator [*Dubosclard et al.*, 2004], or by an eruptive seismic signal of some predefined threshold potentially linked to an alarm system. This option is useful when monitoring isolated explosions interspersed with long intervals of quiet activity, as characteristic of many volcanoes. In addition to the immediate benefits for operational surveillance, the long-term deployment of such radar on active volcanoes would enable to document the variability of eruptive behaviors and to build databases potentially useful for future eruptions. Combination with other ground-based methods, such as visual and infrared imagery, broadband seismic, ultrasound detection and gas analysis would shed light on the complex interactions among various eruptive processes. Thermal video such as Forward Looking Infrared Radiometer (FLIR) would be particularly helpful for the study of Strombolian activity. Its capacity to detect both fine ash plumes and large blocks can bring additional constraints on PSDs. This method can also provide further insights on Strombolian source conditions [*Patrick et al.*, 2007]. Besides, our methodology of particle loading estimation could be extended to the study and monitoring of volcanic ash plumes. With this aim, the coupling of multichannel satellite imagery with ground-based radar measurements would be particularly relevant for the mitigation of risks related to ash clouds and for the investigations on ash plume dynamics.

Appendix A: Electromagnetic Scattering Equations

[41] Considering the wide range of particle diameters characterizing volcanic activity, the complete scattering theory is required to account for the effects of large particles. A general solution of electromagnetic wave scattering was given by *Mie* [1908]. The derivation of the electromagnetic scattering model specifically applied to the case of volcanic studies is developed in this section. In this first approach of scattering by volcanic ejecta, we apply Maxwell's equations for plane wave scattered by spherical particles in a homogeneous medium at a large distance [e.g., *Bohren and Huffman*, 1983].

[42] Starting with Maxwell's equation for plane waves:

$$\nabla \cdot E = 0 \tag{A1}$$

$$\nabla \cdot H = 0 \tag{A2}$$

$$\nabla \times E = i\omega\mu H \tag{A3}$$

$$\nabla \times H = -i\omega\varepsilon E \tag{A4}$$

where E and H are the electric and magnetic fields. ε is the dielectric permittivity, μ is the magnetic permeability, and ω is angular frequency. Taking the curl of (A3) and (A4), gives:

$$\begin{aligned} \nabla \times (\nabla \times E) &= i\omega\mu\nabla \times H = \omega^2\varepsilon\mu E \\ \nabla \times (\nabla \times H) &= -i\omega\varepsilon\nabla \times E = \omega^2\varepsilon\mu H \end{aligned} \tag{A5}$$

If we use the vector identity,

$$\nabla \times (\nabla \times A) = \nabla(\nabla \bullet A) - \nabla \bullet (\nabla A) \tag{A6}$$

we obtain

$$\nabla^2 E + \omega^2\varepsilon\mu E = 0 \quad \nabla^2 H + \omega^2\varepsilon\mu H = 0 \tag{A7}$$

where $\nabla^2 A = \nabla \cdot (\nabla A)$. Thus, E and H satisfy the wave equation. The field inside the particle is denoted by (E_1, H_1); the field in the medium surrounding the particle (E_2, H_2) is the superposition of the incident field (E_i, H_i) and the scattered field (E_s, H_s):

$$E_2 = E_i + E_s \quad H_2 = H_i + H_s \tag{A8}$$

The electromagnetic field is required to satisfy the Maxwell equations at points where ε and μ are continuous. However, there is a discontinuity at the boundary of the particle, where the following conditions on the fields are imposed:

$$\begin{aligned} [H_2(x) - H_1(x)] \times n_s &= 0 \\ [E_2(x) - E_1(x)] \times n_s &= 0 \end{aligned} \tag{A9}$$

where n_s is the outward directed normal to the surface of the particle. Under the conditions of our study (far-field region and spherical particle), the scattered field E_s is mainly transverse and can be resolved into components parallel ($E_{//}$) and perpendicular ($E_\perp$) to the scattering plane. The relationship between incident and scattered field amplitudes can be written in matrix form:

$$\begin{pmatrix} E_{//s} \\ E_{\perp s} \end{pmatrix} = \frac{e^{ik_n(R-r_z)}}{-ik_nR} \begin{pmatrix} S_2 & 0 \\ 0 & S_1 \end{pmatrix} \begin{pmatrix} E_{//i} \\ E_{\perp i} \end{pmatrix} \tag{A10}$$

where $k_n = 2\pi/\lambda$ is the wave number, R, the distance to the particle, and r_z, the component of R on the direction of propagation of the incident wave. The radiation of an electromagnetic wave can be described in terms of intensity from the four Stokes parameters (I, Q, U, V) describing the various states of polarization: not polarized (I), polarized horizontally ($+Q$), polarized vertically ($-Q$), polarized at $+45°$ ($+U$), polarized at $-45°$ ($-U$), right circularly polarized ($+V$) or left circularly polarized ($-V$). The relationship between incident and scattered Stokes parameters (indexed i and s, respectively) follows from the amplitude scattering matrix, also called the Mueller matrix [*Bohren and Huffman*, 1983; *Wolf and Voshchinnikov*, 2004]:

$$\begin{pmatrix} I_s \\ Q_s \\ U_s \\ V_s \end{pmatrix} = \frac{\lambda^2}{4\pi^2R^2} \begin{pmatrix} S_{11}(\Theta) & S_{12}(\Theta) & 0 & 0 \\ S_{12}(\Theta) & S_{11}(\Theta) & 0 & 0 \\ 0 & 0 & S_{33}(\Theta) & S_{34}(\Theta) \\ 0 & 0 & -S_{34}(\Theta) & S_{33}(\Theta) \end{pmatrix} \begin{pmatrix} I_1 \\ Q_i \\ U_i \\ V_i \end{pmatrix} \tag{A11}$$

The scattering matrix elements ($S_{i,j}$) depend on Θ, which is the angle between the direction of the incident and the scattered radiation of wavelength λ. VOLDORAD transmits power through a square array of four Yagi antennas, such that the incident wave has a horizontal linear polarization ($I_i = 1$, $Q_i = 1$, $U_i = 0$, $V_i = 0$). Thus, in our case, we denote by $i_{//}$ the corresponding scattered irradiance that only depends on the two first scattering matrix elements (S_{11}, S_{12}):

$$i_{//} = S_{11} + S_{12} = |S_2|^2 \tag{A12}$$

with

$$\begin{aligned} S_{11}(\Theta) &= \tfrac{1}{2}\left(|S_2(\Theta)|^2 + |S_1(\Theta)|^2\right) \\ S_{12}(\Theta) &= \tfrac{1}{2}\left(|S_2(\Theta)|^2 - |S_1(\Theta)|^2\right) \end{aligned} \tag{A13}$$

The sum of the two first scattering matrix elements can then be derived from the single complex amplitude function S_2 in the form of a convergent series:

$$S_2(\Theta) = \sum_{n=1}^{\infty} \frac{2n+1}{n(n+1)} \left(a_n\tau_n(\Theta) + b_n\pi_n(\Theta)\right) \tag{A14}$$

where n is a positive integer, a_n and b_n are the complex scattering coefficients (Mie coefficients), and τ_n and π_n are the angular functions. The series can be terminated after n_c sufficiently large terms. The complex scattering coefficients depend particularly on the size parameter x and the refractive index m of the material [*Sauvageot*, 1992] and are defined as

$$\begin{aligned} a_n &= \frac{m\psi_n(mx)\psi_n'(x) - \psi_n(x)\psi_n'(mx)}{m\psi_n(mx)\xi_n'(x) - \xi_n(x)\psi_n'(mx)} \\ b_n &= \frac{\psi_n(mx)\psi_n'(x) - m\psi_n(x)\psi_n'(mx)}{\psi_n(mx)\xi_n'(x) - m\xi_n(x)\psi_n'(mx)} \end{aligned} \tag{A15}$$

The size parameter $x = k_{nr}$ is a dimensionless variable, r, being the radius of the spherical particle. Ψ and ξ are the Riccati-Bessel functions of first and second kind and can be defined by

$$\begin{aligned} \psi_n(x) &= xj_n(x) \\ \xi_n(x) &= j_n(x) + iy_n(x) \end{aligned} \tag{A16}$$

where j_n and y_n are the spherical Bessel functions of first and second kind defined as

$$\begin{aligned} j_n(x) &= \sqrt{\tfrac{\pi}{2x}} J_{n+1/2}(x) \\ y_n(x) &= \sqrt{\tfrac{\pi}{2x}} Y_{n+1/2}(x) \end{aligned} \tag{A17}$$

The spherical Bessel functions satisfy the recurrence relations:

$$\begin{aligned} z_{n-1}(x) + z_{n+1}(x) &= \tfrac{2n+1}{x} z_n(x) \\ (2n+1)\tfrac{d}{dp} z_n(x) &= nz_{n-1}(x) - (n+1)z_{n+1}(x) \end{aligned} \tag{A18}$$

The angular functions τ_n and π_n depend only on Θ and are defined by the Legendre polynomials,

$$\begin{aligned} \pi_n(\Theta) &= \frac{P_n^1(\Theta)}{\sin\Theta} \\ \tau_n(\Theta) &= \frac{dP_n^1(\Theta)}{d\Theta} \end{aligned} \tag{A19}$$

and can be found from the recurrence relations:

$$\begin{aligned} \tau_n(\Theta) &= n\cos\Theta\pi_n(\Theta) - (n+1)\pi_{n-1}(\Theta) \\ \pi_n(\Theta) &= \tfrac{2n-1}{n-1}\cos\Theta\pi_{n-1}(\Theta) - \tfrac{n}{n-1}\pi_{n-2}(\Theta) \end{aligned} \tag{A20}$$

The scattered irradiance can now be calculated for any particle size, under the special conditions of our sounding using VOLDORAD at Mount Etna (Figure 1). Determining the scattering matrix elements enables us to define the scattering cross section of each particle; this then relates irradiance to reflectivity through the Mie coefficients. VOLDORAD is a monostatic radar (i.e., the same antenna is used for transmission and reception), thus we define a

backscattering cross section (σ_{bks}) for horizontal linear polarization:

$$\sigma_{bks} = \frac{\lambda^2}{4\pi}\left|\sum_{n=1}^{\infty}(-1)^2(2n+1)(a_n - b_n)\right|^2 \quad \text{(A21)}$$

Note that we often use the backscattering efficiency defined as the cross section coefficient normalized by the particle section such as

$$Q_{bks} = \frac{\sigma_{bks}}{\pi r^2} \quad \text{(A22)}$$

The theoretical radar power for a distributed target in a sampling volume (V_s) at a given distance (R) can then be deduced from the radar reflectivity (η), which is simply the sum of the backscattering cross section (σ_{bks}) of each particle over a unit volume [*Doviak and Zrnic*, 1984; *Sauvageot*, 1992],

$$P_{synth} = \frac{C_r V_s \eta}{R^4} \quad \text{(A23)}$$

$$\eta = \sum_{i=1}^{n}\frac{\sigma_{bks}}{V_s} \quad \text{(A24)}$$

where C_r is the radar constant defined by a set of technical parameters related to the radar configuration.

Notation

α radar beam width (deg).
A_0 amplitude of electromagnetic wave.
a_n, b_n complex scattering coefficients (magnetic and electric mode).
B_r noise of Doppler spectrum (mW).
C mass particle concentration (kg m^{-3}).
C_c constant of conversion.
C_d drag coefficient.
C_p magma specific heat capacity (J kg^{-1} K^{-1}).
C_r radar constant (mW m^2).
C_s shape coefficient of a spherical particle.
D diameter of particle (m).
D_L validity limit diameter (m).
D_p average particle diameter (m).
Δt_{cross} duration for the jet to cross a range gate (s).
Δt_{jet} duration of jet production (s).
E,H electric and magnetic fields (N C^{-1}; A m^{-1}).
ε dielectric permittivity (F m^{-1}).
E_k kinetic energy (J).
E_T thermal energy (J).
f_d Doppler frequency (Hz).
f_t transmitted frequency (Hz).
f_w scaled Weibull probability density function.
γ range of the particle size distribution (m).
G_n range gates (sampling volume).
η radar reflectivity (cm^{-1}).
$i_{//}$ parallel scattered irradiance (W m^{-2}).
j_n, y_n spherical Bessel functions of first and second kind.
K complex dielectric factor.
k shape factor.
k_n wave number (rad m^{-1}).
Λ shift factor.
L length of the range gate (m).
m complex refractive index.
M mass of particles (kg).
μ magnetic permeability (H m^{-1}).
μ_n mode of the particle size distribution (m).
∇ vector differential operator (nabla symbol).
$\nabla \bullet A$ divergence of a vector field A.
$\nabla \times A$ curl of a vector field A.
$\nabla^2 A$ Laplacian of a vector field A.
N number of particles.
N_c number of coherent integrations of radar pulses.
N_{max} scale factor.
N_t characteristic Number of Doppler spectra.
ω angular frequency (rad s^{-1}).
$P_{\pm}$ radar power received (mW).
P_{mes} radar raw power received (mW).
P_{synth} radar synthetic power received (mW).
P_t peak power (W).
P_{tot} total radar power received (mW).
Θ angle between incident and scattered radiation (deg).
θ antenna beam elevation angle (deg).
Q_{bks} backscattering efficiency.
r radius of the particle (m).
R slant distance between radar and target (m).
r_z component of R on the incident wave direction.
ρ_a, ρ_p densities of air and particles (kg m^{-3}).
σ_{bks} backscattering cross section (m^2).
$S(v)$ power spectral density.
S_2 complex amplitude function (parallel component).
S_{11}, S_{12} scattering Mueller matrix elements.
S_w scaled Weibull distribution.
τ pulse duration (μs).
π_n, τ_n angular functions.
T magma temperature (K).
t_r pulse repetition period (μs).
V volume of pyroclasts (m^3).
$\bar{V}^{+}_{max}$ average maximum velocity of ejected pyroclasts (m s^{-1}).
$V^{\pm}_{max}$ maximum velocities of ejected pyroclasts (m s^{-1}).
$V^{\pm}_{mean}$ mean velocities of ejected pyroclasts (m s^{-1}).
V_r radial velocity of ejected pyroclasts (m s^{-1}).
V_s radar sampling volume (m^3).
x size parameter.
X vector of variable input parameters.
ψ, ξ Riccati–Bessel functions of first and second kind.
Z radar reflectivity factor (mm^6 m^{-3}).
λ radar wavelength (cm).
$(I,Q,U,V)_{i,s}$ incident and scattered Stokes parameters (polarization state).

[43] **Acknowledgments.** We acknowledge Geoff Wadge and an anonymous reviewer for their thoughtful reviews that significantly enhanced this

paper, and we thank Richard Arculus and Michael P. Ryan for handling the paper. We also thank T. H. Druitt for his insightful comments that considerably improved the manuscript and S. Vergniolle for discussions on this topic. Georges Dubosclard, Roland Cordesses, and Claude Hervier are especially acknowledged for the precious radar measurements carried out in the field, without which this work could not have been achieved. M. Gouhier's Ph.D. work was supported by a French MESR fellowship. Field work on Etna was possible thanks to the logistical help of the INGV Catania and was funded by the CNRS-INSU PNRN programs 1999–2001.

References

Adams, R. J., W. F. Perger, W. I. Rose, and A. Kostinski (1996), Measurements of the complex dielectric constant of volcanic ash from 4 to 19 GHz, *J. Geophys. Res.*, *101*, 8175–8185, doi:10.1029/96JB00193.

Bohren, C. F., and D. R. Huffman (1983), *Absorption and Scattering of Light by Small Particles*, 489 pp., Wiley-Interscience, New York.

Carn, S. A., A. J. Prata, and S. Karlsdóttir (2008), Circumpolar transport of a volcanic cloud from Hekla (Iceland), *J. Geophys. Res.*, *113*, D14311, doi:10.1029/2008JD009878.

Chouet, B., N. Hamisevicz, and T. R. McGetchin (1974), Photoballistics of Volcanic Jet Activity at Stromboli, Italy, *J. Geophys. Res.*, *79*, 4961–4976, doi:10.1029/JB079i032p04961.

Dean, K., S. A. Bowling, G. Shaw, and H. Tanaka (1994), Satellite analyses of movement and characteristics of the Redoubt Volcano plume, *J. Volcanol. Geotherm. Res.*, *62*, 339–352, doi:10.1016/0377-0273(94)90040-X.

Dehn, J., K. Dean, and K. Engle (2000), Thermal monitoring of North Pacific volcanoes from space, *Geology*, *28*, 755–758, doi:10.1130/0091-7613(2000)28<755:TMONPV>2.0.CO;2.

Donnadieu, F., G. Dubosclard, R. Cordesses, T. Druitt, C. Hervier, J. Kornprobst, J. F. Lénat, P. Allard, and M. Coltelli (2005), Remotely monitoring volcanic activity with ground-based Doppler radar, *Eos Trans. AGU*, *86*, 204, doi:10.1029/2005EO210001.

Doviak, R. J., and D. S. Zrnic (1984), *Doppler Radar and Weather Observations*, 562 pp., Academic, Orlando, Fla.

Dubosclard, G., R. Cordesses, P. Allard, C. Hervier, M. Coltelli, and J. Kornprobst (1999), First testing of a volcano Doppler radar (Voldorad) at Mt. Etna, *Geophys. Res. Lett.*, *26*, 3389–3392, doi:10.1029/1999GL008371.

Dubosclard, G., F. Donnadieu, P. Allard, R. Cordesses, C. Hervier, M. Coltelli, M. Privitera, and J. Kornprobst (2004), Doppler radar sounding of volcanic eruption dynamics at Mount Etna, *Bull. Volcanol.*, *66*, 443–456, doi:10.1007/s00445-003-0324-8.

Francalanci, L., P. Manetti, and A. Pecerillo (1989), Volcanological and magmatological evolution of Stromboli volcano (Aeolian islands): The roles of fractional crystallization, magma mixing, crustal contamination and source heterogeneity, *Bull. Volcanol.*, *51*, 355–378, doi:10.1007/BF01056897.

Gouhier, M., and F. Donnadieu (2006), Numerical modeling of Doppler radar signals of Strombolian eruptions, *Eos Trans. AGU*, *87*(52), Fall Meet. Suppl., Abstract V43B-1794.

Harris, D. M., and W. I. Rose (1983), Estimating particles size, concentrations, and total mass of ash in volcanic clouds using weather radar, *J. Geophys. Res.*, *88*, 10,969–10,983, doi:10.1029/JC088iC15p10969.

Harris, D. M., W. I. Rose, R. Roe, and M. R. Thompson (1981), Radar observations of ash eruptions, *U.S. Geol. Surv. Prof. Pap.*, *1250*, 323–333.

Hort, M., and R. Seyfried (1998), Volcanic eruption velocities measured with a micro radar, *Geophys. Res. Lett.*, *25*, 113–116.

Hort, M., R. Seyfried, and M. Vöge (2003), Radar Doppler velocimetry of volcanic eruptions: Theoritical considerations and quantitative documentation of changes in eruptive behaviour at Stromboli, Italy, *Geophys. J. Int.*, *154*, 515–532, doi:10.1046/j.1365-246X.2003.01982.x.

Kittleman, L. R. J. (1964), Application of Rosin's distribution in size frequency analysis of clastic rocks, *J. Sediment. Petrol.*, *34*, 483–502.

Krotkov, N. A., et al. (2008), Validation of SO_2 retrievals from the Ozone Monitoring Instrument over NE China, *J. Geophys. Res.*, *113*, D16S40, doi:10.1029/2007JD008818.

Lacasse, C., S. Karlsdóttir, G. Larsen, H. Soosalu, W. I. Rose, and G. G. J. Ernst (2004), Weather radar observations of the Hekla 2000 eruption cloud, Iceland, *Bull. Volcanol.*, *66*, 457–473, doi:10.1007/s00445-003-0329-3.

Marzano, F. S., G. Vulpiani, and W. I. Rose (2006a), Microphysical characterization of microwave radar reflectivity due to volcanic ash clouds, *IEEE Trans. Geosci. Remote Sens.*, *44*, 313–327, doi:10.1109/TGRS.2005.861010.

Marzano, F. S., S. Barbieri, G. Vulpiani, and W. I. Rose (2006b), Volcanic ash cloud retreival by ground-based microwave weather radar, *IEEE Trans. Geosci. Remote Sens.*, *44*, 3235–3246, doi:10.1109/TGRS.2006.879116.

McGetchin, T. R., M. Settle, and B. Chouet (1974), Cinder cone growth modeled after northeast crater, Mount Etna, Sicily, *J. Geophys. Res.*, *79*, 3257–3272, doi:10.1029/JB079i023p03257.

Mie, G. (1908), Beiträge zur Optik trüber Medien, speziell kolloidaler Metallösungen, *Ann. Phys.*, *330*(3), 377–445.

Nakamura, Y. (1984), The 1888 eruption of Bandai volcano, Japan: Grain size distribution, paper presented at IAVCEI Meeting, Int. Assoc. of Volcanol. and Chem. of the Earth's Interior, Rome, 13–17 Aug.

Patrick, M. R., A. J. L. Harris, M. Ripepe, J. Dehn, D. A. Rothery, and S. Calvari (2007), Strombolian explosive styles and source conditions: Insights from thermal (FLIR) video, *Bull. Volcanol.*, *69*, 769–784, doi:10.1007/s00445-006-0107-0.

Pointin, Y., J. Fournet-Fayard, and F. Donnadieu (2005), Calibration du radar UHF VOLDORAD 2, par comparaison de ses données avec celles du disdromètre du LaMP/OPGC., *Note OPGC 144*, 61 pp., Obs. de Phys. du Globe, Clermont-Ferrand, France.

Riley, C. M., W. I. Rose, and G. J. S. Bluth (2003), Quantitative shape measurements of distal volcanic ash, *J. Geophys. Res.*, *108*(B10), 2504, doi:10.1029/2001JB000818.

Ripepe, M., M. Rossi, and G. Saccorotti (1993), Image processing of explosive activity at Stromboli, *J. Volcanol. Geotherm. Res.*, *54*, 335–351, doi:10.1016/0377-0273(93)90071-X.

Rogers, R., and M. Yau (1989), *A Short Course on Cloud Physics*, Pergamon, Oxford, U.K.

Sauvageot, H. (1992), *Radar Meteorology*, 366 pp., Artech House, Boston, Mass.

Self, S., R. S. J. Sparks, B. Booth, and G. P. L. Walker (1974), The 1973 Heimaey Strombolian Scoria deposit, Iceland, *Geol. Mag.*, *111*, 539–548.

Seyfried, R., and M. Hort (1999), Continuous monitoring of volcanic eruption: A review of various techniques and new results from a frequency-modulated radar Doppler system, *Bull Volcanol.*, *60*, 627–639.

Sheridan, M. F. (1971), Particle-size characteristics of pyroclastic tuffs, *J. Geophys. Res.*, *76*, 5627–5634, doi:10.1029/JB076i023p05627.

Sheridan, M. F., K. H. Wohletz, and J. Dehn (1987), Discrimination of grain-size subpopulations in pyroclastic deposits, *Geology*, *15*, 367–370, doi:10.1130/0091-7613(1987)15<367:DOGSIP>2.0.CO;2.

Spieler, O., M. Alidibirov, and D. B. Dingwell (2003), Grain-size characteristics of experimental pyroclasts of 1980 Mount St. Helens cryptodome dacite: Effects of pressure drop and temperature, *Bull. Volcanol.*, *65*, 90–104.

Vosteen, H. D., and R. Schellschmidtb (2003), Influence of temperature on thermal conductivity, thermal capacity and thermal diffusivity for different types of rock, *Phys. Chem. Earth*, *28*, 499–509.

Watson, I. M., V. J. Realmuto, W. I. Rose, A. J. Prata, G. J. S. Bluth, Y. Gu, C. E. Bader, and T. Yu (2004), Thermal infrared remote sensing of volcanic emissions using the moderate resolution imaging spectroradiometer, *J. Volcanol. Geotherm. Res.*, *135*, 75–89, doi:10.1016/j.jvolgeores.2003.12.017.

Weibull, W. (1939), A statistical theory of the strength of materials, *R. Swed. Inst. Eng. Res.*, *151*.

Weill, A., G. Brandeis, S. Vergniolle, F. Baudin, J. Bilbille, J. F. Fèvre, B. Piron, and X. Hill (1992), Acoustic sounder measurements of the vertical velocity of volcanic jets at Stromboli volcano, *Geophys. Res. Lett.*, *19*, 2357–2360, doi:10.1029/92GL02502.

Williams, H., and A. R. McBirney (1979), *Volcanology*, 397 pp., Freeman Cooper, San Francisco, Calif.

Wohletz, K. H., M. F. Sheridan, and W. K. Brown (1989), Particle size distributions and the sequential fragmentation/transport theory applied to volcanic ash, *J. Geophys. Res.*, *94*, 15,703–15,715, 721, doi:10.1029/JB094iB11p15703.

Wolf, S., and N. V. Voshchinnikov (2004), Mie scattering by ensembles of particles with very large size parameters, *Comput. Phys. Commun.*, *162*, 113–123, doi:10.1016/j.cpc.2004.06.070.

Woods, A. W., and M. I. Bursik (1991), Particle fallout, thermal disequilibrium and volcanic plumes, *Bull. Volcanol.*, *53*, 559–570, doi:10.1007/BF00298156.

F. Donnadieu and M. Gouhier, Laboratoire Magmas et Volcans (UMR 6524 CNRS-IRD), 5, rue Kessler, F-63038 Clermont-Ferrand, France. (F.Donnadieu@opgc.univ-bpclermont.fr; M.Gouhier@opgc.univ-bpclermont.fr)